CEAI, Vol.24, No. 3, pp. 12-20, 2022 Printed in Romania

Adaptive Model Predictive Control for Switching Frequency Reduction of Transformerless Inverter-based Systems

Abdulrahman J. Babqi *

* *Department of Electrical Engineering, College of Engineering, Taif University, KSA, P. O. Box 11099, Taif 21944, Saudi Arabia (E-mail: ajbabqi@tu.edu.sa)*

Abstract: In this paper, an adaptive finite control set model predictive control (AFCS-MPC) for switching frequency reduction of transformerless inverters is proposed. The new control method improves the conventional finite control set model predictive control (FCS-MPC) applications in PV system control. The AFCS-MPC does not require using weighting factors as well as no need for external modulation. The idea of the proposed control strategy is to implement a long prediction horizon during steady-state or in the case of a small variation between the reference and controlled variable. On the other hand, in the case of a large dynamic change between the reference and controlled variable, the controller predicts only the first step. In this manner, the controller guarantees the performance of FCS-MPC with a reduced switching frequency. The proposed control method is capable of reducing the average switching frequency of the conventional finite control set model predictive control as per numerous simulation observations. Simulation results are presented using PSCAD/EMTDC platform to verify the performance of the proposed method compared to the standard FCS-MPC.

Keywords: Adaptive Model Predictive Control, switching frequency reduction, transformerless, power electronics, distributed generation.

1. INTRODUCTION

Renewable energy sources (RESs), such as solar, wind, biomass, etc., can be powerful energy source alternatives for conventional fossil fuels Nassif and Long (2016). According to REN21's annual Renewable Global Status Report-2021 Ranalder et al. (2020), more than 256 GW of renewable energy capacity was installed in 2020. The solar photovoltaic (PV) accounted for more than 139 GW of the newly installed renewable energy capacity followed by wind power. Moreover, the total global solar PV capacity was 627 GW by the end of 2019. However, solar PV systems like most renewable energy sources are intermittent, and integrating these sources into the existed electric power grids presents several major technical issues Naeem and Hassan (2020); Wang et al. (2018). Another concern with PV solar systems is the variability of the output power which depends on natural conditions such as irradiance intensity, clouds, or dust. Power electronics devices (PEDs) such as inverters have been playing a key role in solar PV systems integration Nikoletatos and Tselepis (2015). Besides interfacing PV systems into electrical grids, inverters enable advanced control techniques. They can provide flexible active and reactive power flow, voltage and frequency stability service, power factor corrections, PV maximum power point tracking, and fault ride-through capability Yi et al. (2018); Yi and Etemadi (2017); Jafarian et al. (2018).

In general, grid-connected PV systems can be categorized into two types: 1) transformer-isolated and 2) transformerless PV systems. Besides stepping the voltage up or down, transformers provide galvanic isolation which eliminates the common-mode voltage (CMV) and leakage current generated by the high voltage switching inverters Kwak and Mun (2014); Hou et al. (2012); Xie et al. (2017); Huang et al. (2021); Long et al. (2015). Since transformers are costly, large in size, and inefficient, transformerless PV systems are preferred when voltage levels can be met Shayestegan (2018). Especially, in residential and commercial/industrial PV systems, most PV inverter connects to the point of interconnection (POI) without an inverter. However, the lack of galvanic isolation can create an electrical path between the PV and grid, resulting in leakage current. Moreover, parasitic capacitance can be formed when the PV is grounded which would raise safety issues for operators. Therefore, different inverter topologies such as H5 and H7 inverters have been proposed in the literature recently to overcome these issues Guo et al. (2017); Li et al. (2018); Kumar et al. (2020); Freddy et al. (2014). The H5 inverter topology was proposed in Victor et al. (2008) where an extra switch was added in series with the DC source (i.e., PV panel) of the conventional full-bridge single-phase inverter. The purpose of the extra switch is to isolate the PV panel in zero operation mode. Therefore, the CMV and leakage current are reduced. Similarly, the H7 inverter is a modified topology of the three-phase two-level inverter by adding one more switch. In Guo et al. (2017), the authors proposed a new modulation technique for leakage current attenuation reduction of a cascade three-phase H5 inverter. The work was compared with the full-bridge single-phase inverter. For further CMV reduction, a new topology of the H5 inverter was proposed in Li et al. (2018). The proposed topology was capable of reducing the CMV by two-thirds of the original H5. A bidirectional clamping-based topology of different transformerless inverters was proposed in Kumar et al. (2020). The topology reduces the CMV as well as the leakage current. In Freddy et al. (2014), the performance of the H7 inverter was investigated in reducing the CMV and leakage current using a modified discontinuous pulse-width modulation technique.

Different control strategies have been used for controlling inverter-based PV solar systems. In the past decade, finite control set model predictive control (FCS-MPC) has been getting more attention as a promising strategy for controlling PEDs since it provides many advantages including generating the switching signals internally, fast dynamics response, constraints being included in the cost function, the ease of implementing, and simultaneous multi-objective parameters control Rodriguez and Cortes (2012); Yi et al. (2019). However, few works have implemented FCS-MPC for H5 and H7 inverters Babqi et al. (2018); Jung et al. (2018). FCS-MPC was proposed for extracting the maximum power point of the PV system using the H5 inverter in Babqi et al. (2018) while a current control of a modified H7 topology using FCS-MPC was proposed in Jung et al. (2018). A Comprehensive comparison between FCS-MPC and proportional-integral control for controlling different grid-connected PEDs was presented by Babqi and Alamri (2021). The work compares the performance of the two controllers in terms of leakage current, total harmonics distortion, switching frequency, common-mode voltage, and steady-state error during grid-connected operation. However, the high switching frequency generated by the FCS-MPC might become a burden for the inverter.

One of the main drawbacks of conventional FCS-MPC is the requirement of a high switching frequency. Multiple FCS-MPC switching frequency reduction techniques have been proposed in the literature. A predictive technique is proposed in Vargas et al. (2014) to maintain the switching frequency as well as mitigate the common-mode voltage of an induction machine. Authors in Rodriguez et al. (2012) explain the capability of the FCS-MPC multi-objective parameters control (e.g., switching frequency reduction) for different power electronics devices. A minimized switching states model predictive control was proposed in Li et al. (2015) for a single-phase grid-connected inverter. The aforementioned works reduced the FCS-MPC switching frequency by adding one term in the cost function which acts as a constraint. Even though these works showed a significant reduction in the output FCS-MPC switching frequency, it is a time-consuming process and required much effort to adjust the weighting factor in the cost function. A multi-step finite control set model predictive control with reference tracking and long prediction horizons was proposed in Geyer and Quevedo (2014). However, the multi-step prediction increased the computational burdens which make the method time-consuming and increases computation burden. In Cortes et al. (2010); Hu et al. (2014), a two-step prediction horizon was proposed to improve FCS-MPC performance. However, the method provides a small switching frequency reduction and requires an accurate system model. A low switching frequency-based predictive control for grid-connected inverter was proposed in Sangsefidi et al. (2016). The method used two different cost functions for both steady-state and transient responses. However, the use of the weighting factor increases the complexity of the control method. As an attempt to address the aforementioned drawbacks, this paper proposes an adaptive finite control set model predictive control (AFCS-MPC) for switching frequency reduction of grid-connected transformerless solar PV systems. There is no need for using weighting factors in the cost function unless any constraints are added in the cost function such as over current protection. Moreover, the switching states generate internally similar to conventional FCS-MPC and there is no need for external modulations. The main contribution of this work include the following:

(1) A unified FCS-MPC designing process for transformerless PV systems including H5 and H7 inverters.
(2) A new switching frequency reduction method, the AFCS-MPC algorithm, is proposed and validated.
(3) Case studies on the AFCS-MPC for H5, three-phase H5, and H7 inverters with proven performance.

The rest of the paper is organized as follows. Section 2 explains generalized FCS-MPC for power electronics control. Section 3 introduces the proposed AFCS-MPC for transformerless PV systems. Section 4 presents the case studies that verify the proposed method. Section 5 concludes the paper.

2. GENERALIZED FINITE CONTROL SET MODEL PREDICTIVE CONTROL FOR TRANSFORMERLESS PV SYSTEMS

Model predictive control (MPC) is a control strategy based on an optimization process that uses the system model to predict the future values of the controlled parameters. Since power converters generate a finite number of output voltage vectors, MPC can be called finite control set model predictive control which reduces the prediction process to only those possible switching states corresponding to the controlled power electronic device Kouro et al. (2008). In order to implement FCS-MPC, a system state-space model can be firstly derived

$$\begin{aligned} \dot{x}(t) &= A\, x(t) + B\, u(t) \\ y(t) &= C\, x(t) + D\, u(t) \end{aligned} \tag{1}$$

where x is a state vector column n, $x(t) \in \mathbb{R}^n$, and y is an output vector column m, $y(t) \in \mathbb{R}^m$. u is an input or control vector column r, $u(t) \in \mathbb{R}^r$. A and B are the system and input matrices with dimensions of $n \times n$ and $n \times r$, respectively. C is the output matrix with $m \times n$ dimensions while D is the feedforward $m \times r$ matrix. Predicting the future values of the states using FCS-MPC requires obtaining the system discrete-time model. One method to derive the discrete-time model of a system is the finite difference approximation method Babqi and Etemadi (2017):

$$\dot{x}(t) \simeq \frac{x(k+1) - x(k)}{T_s} \tag{2}$$

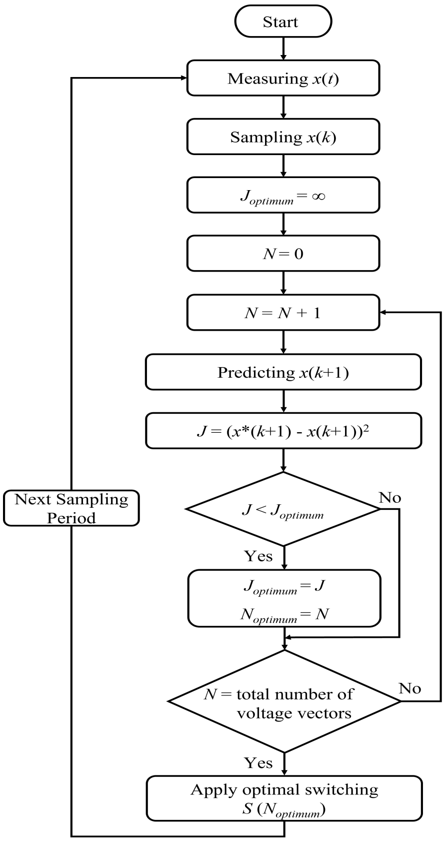

Fig. 1. Conventional FCS-MPC Flowchart

where $x(k+1)$ is the one step ahead of the future value of the controlled state, $x(k)$ is the present value, and T_s is the sampling time. Substituting (2) in (1), the system discrete state-space model is:

$$\begin{aligned} x(k+1) &= A_d\ (k) + B_d\ u(k) \\ y(k) &= C_d\ x(k) + D_d\ u(k) \end{aligned} \tag{3}$$

where A_d, B_d, C_d, and D_d are the matrices associated with the system discrete state-space model, and

$$\begin{aligned} A_d &= e^{AT_s}, \\ B_d &= \int_0^{T_S} e^{A\tau} B\, d\tau, \\ C_d &= C,\ D_d = D. \end{aligned} \tag{4}$$

For a small sampling time T_s, the exponential matrix can be approximated as:

$$\begin{aligned} e^{AT_s} &= 1 + AT_s + \frac{(AT_s)^2}{2!} + \frac{(AT_s)^3}{3!} + \ldots + \frac{(AT_s)^n}{n!} \\ e^{AT_s} &\simeq 1 + AT_s \end{aligned} \tag{5}$$

As mentioned previously in this section, the power electronics devices produce a finite number of voltage vectors which are used as inputs ($u(k)$) to the system. Therefore, a cost function (6) is used to evaluate each voltage vector and select the optimal one that results in the lowest error between the reference and predicted values where $x^*(k+1)$ is the reference value. As a result, a combination of actuation signals corresponding to the optimal value that is selected by the cost function is sent to the power converter. Fig. 1 illustrates the procedure of the FCS-MPC process.

$$J = (x^*(k+1) - x(k+1))^2 \tag{6}$$

The control can be performed using short prediction horizon (i.e. $x(k+1)$) or longer ones (i.e. $x(k+2)$, $x(k+3)$, ..., $x(k+n)$) which are called long prediction horizons. FCS-MPC control scheme requires solving a large number of computational equations, especially in cases such as cascaded and three-phase typologies. As a result, a short prediction horizon introduces a considerable time delay between the measurements and the actuation that is sent to the power electronic device Cortes et al. (2011). Moreover, since the average switching frequency of FCS-MPC is not fixed, using one-step prediction will usually be performed on high switching frequency, thus increasing the switching burdens of the semiconductor switches and reducing their life span. On the other hand, predicting a longer horizon improves the performance of the controller Geyer (2011). It allows the FCS-MPC to make a well conversant decision on the optimization process which eliminates the time delay that occurs in short step prediction. It also reduces the switching frequency. Even though implementing a longer horizon is very expensive and computationally challenging, technology development nowadays has made it possible. Therefore, a trade-off between the control performance and sampling time must be considered when selecting the horizon length.

3. ADAPTIVE FCS-MPC FOR SINGLE-PHASE AND THREE-PHASE PV SYSTEMS

The proposed adaptive finite control set model predictive control senses the difference between the measured and reference values. If the difference is larger than a certain limit, the controller implements the short horizon (i.e. $x(k+1)$). On the other hand, if the difference is less than the limit, the controller extends the prediction step to a longer horizon (e.g. $x(k+2)$, $x(k+3)$, ..., $x(k+n)$). In other words, AFCS-MPC implements a longer horizon for the future prediction at steady-state while in dynamic transitions, the controller uses a shorter step for the prediction. In this manner, the AFCS-MPC not only compensates for the time delay but also reduces the switching frequency which is confirmed by the case studies in section 4. Fig. 2 illustrates the process of the proposed AFCS-MPC. The following subsections use several popular transformerless PV inverters as examples to show how AFCS-MPC is designed and working on these topologies. Note that other topologies are also applicable with proper derivation and controller design.

3.1 AFCS-MPC of A Single-phase H5 Inverter

H5 inverter, Fig. 3(a), is a modified version of the full H-bridge inverter by adding one more switch S_5. The additional switch disconnects the PV from the grid during the zero voltage vectors which prevents the freewheeling current from flowing back to the PV terminal. As a result, the leakage current reduces Babqi et al. (2018). Similar to the H-bridge, H5 has four modes of operation but

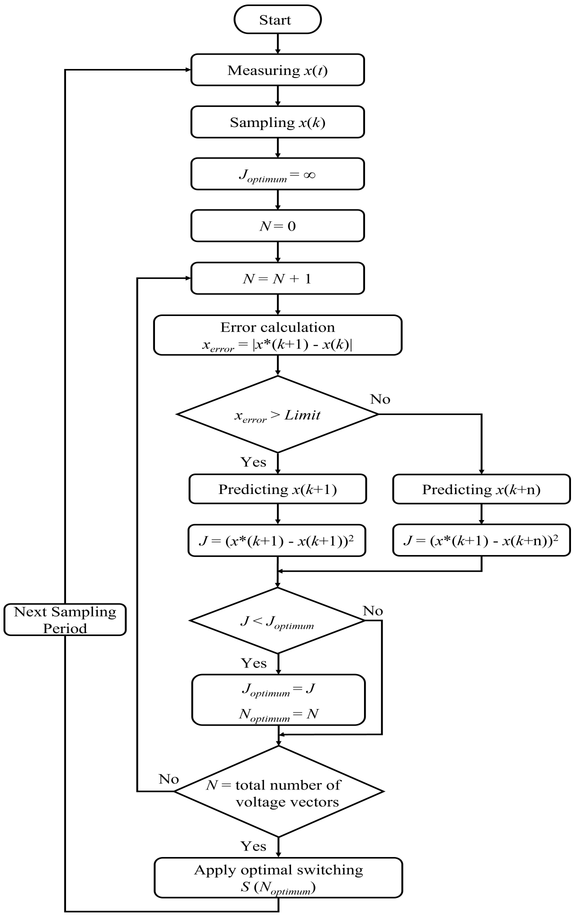

Fig. 2. AFCS-MPC Flowchart

with different switching signals pattern. Table 1 shows the H5 four modes of operations and their corresponding switching states space vectors modulation.

The load current dynamic $i_{f,1}$ in Fig. 3(a) can be derived using KVL in the power circuit as:

$$v_{i,1} = v_{L_{f,1}} + e_1 \tag{7a}$$

$$L_{f,1}\frac{di_{f,1}}{dt} = v_{i,1} - e_1 \tag{7b}$$

$$\frac{di_{f,1}}{dt} = \frac{1}{L_{f,1}}\ (v_{i,1} - e_1) \tag{7c}$$

where $v_{i,1}$ and e_1 are the inverter output and utility grid voltages, respectively. $v_{L,1}$ is the inductor voltage. The discrete time-domain of the load current is obtained by substituting (2) and (4) in (7c) which results in:

$$i_{f,1}(k+1) = i_{f,1}(k) + \frac{T_s}{L_{f,1}}(v_{i,1}(k) - e_1(k)) \tag{8}$$

$i_{f,1}(k+1)$ is the first step prediction of the load current (i.e. short horizon) while $i_{f,1}(k)$ is the present value. $v_{i,1}(k)$ and $e_1(k)$ are the inverter present output and utility grid voltages values, respectively. In order to predict a longer horizon of the load current, the utility grid voltage should be estimated. Note that in one sampling time, utility grid voltage does not change considerably Rodriguez et al. (2007). As a result, it can be assumed that $e_1(k) = e_1(k+1)$. Therefore, the utility grid voltage can be estimated using (8) as:

Table 1. H5 inverter operation modes

Mode	S_1	S_2	S_3	S_4	S_5	V_i
1	1	0	0	1	1	V_{DC}
2	1	0	0	0	0	0
3	0	1	1	0	1	$-V_{DC}$
4	0	0	1	0	0	0

$$e_1(k) = e_1(k+1) = v_{i,1}(k) - \frac{L_{f,1}}{T_s}(i_{f,1}(k+1) - i_{f,1}(k)) \tag{9}$$

using (9), the second step prediction of the load current is:

$$i_{f,1}(k+2) = i_{f,1}(k+1) + \frac{T_s}{L_{f,1}}(v_{i,1}(k) - e_1(k+1)) \tag{10}$$

As a result, the n-step of the load current is predicted as:

$$i_{f,1}(k+n) = i_{f,1}(k+(n-1)) + \frac{T_s}{L_{f,1}}(v_{i,1}(k) - e_1(k+(n-1))) \tag{11}$$

Depending on the difference between the measured, present, current value $i_{f,1}(k)$ and reference values i^*, the proposed AFCS-MPC decides either to predict the first or longer step prediction horizon. In case the difference is larger than a specific limit, the cost function (12) is used. Otherwise, the cost function (13) is used.

$$J = (i^*(k+1) - i_{f,1}(k+1))^2 \tag{12}$$

$$J = (i^*(k+n) - i_{f,1}(k+n))^2 \tag{13}$$

In situations where the reference changes, AFCS-MPC uses each possible voltage vector in table 1 to predict the first step of the load current $i_{f,1}(k+1)$ in (8). Consequently, four future values of $i_{f,1}(k+1)$ will be predicted. Then, the cost function (12) evaluates each predicted value of $i_{f,1}(k+1)$ and selects the one that results in the lowest error which is the optimal voltage vector. Regarding the selected voltage vector, appropriate switching signals are sent to the H5 inverter.

In steady-states, a longer horizon is predicted and (13) is used. Assuming that the prediction step is set to 3 (i.e. $n = 3$), thus (14e) is used to predict the load current. In order to predict the third step of the load current, AFCS-MPC should first predict $i_{f,1}(k+2)$ and then estimate $e_1(k+2)$. The process sequence of predicting $i_{f,1}(k+3)$ is illustrated in (14a-14e).

$$i_{f,1}(k+1) = i_{f,1}(k) + \frac{T_s}{L_{f,1}}(v_{i,1}(k) - e_1(k)) \tag{14a}$$

$$e_1(k) = e_1(k+1) \tag{14b}$$

$$i_{f,1}(k+2) = i_{f,1}(k+1) + \frac{T_s}{L_{f,1}}(v_{i,1}(k) - e_1(k+1)) \tag{14c}$$

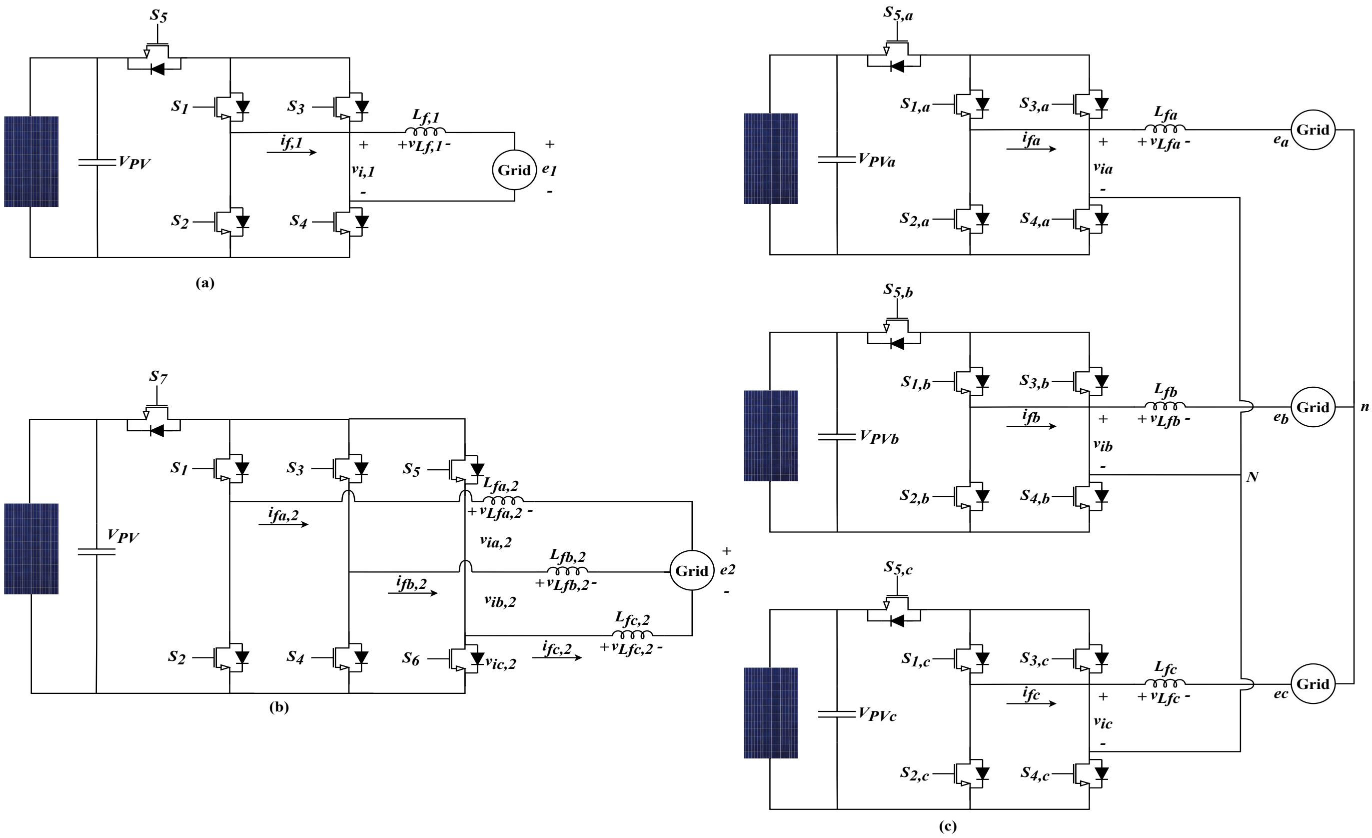

Fig. 3. Studied inverters: (a) H5, (b) three-phase cascaded H5, and (c) three-phase H7

$$e_1(k+2) = v_{i,1}(k) - \frac{L_{f,1}}{T_s}(i_{f,1}(k+2) - i_{f,1}(k+1)) \quad (14d)$$

$$i_{f,1}(k+3) = i_{f,1}(k+2) + \frac{T_s}{L_{f,1}}(v_{i,1}(k) - e_1(k+2)) \quad (14e)$$

Equations (14a) and (14c) are used to predict $i_{f,1}(k+1)$ and $i_{f,1}(k+2)$, respectively. (14d) is used to estimate $e_1(k+2)$. Again, since H5 has four output voltage vectors, AFCS-MPC will predict four values of $i_{f,1}(k+3)$. Finally, the cost function (13) is used to minimize the error and select the optimal voltage vector. Then, the corresponding gating signals of the chosen voltage vector are sent to the H5 inverter. It should be noted that these controlling processes occur in one sampling time either the AFCS-MPC decided to implement a short prediction step (12) or the longer steps (13).

3.2 AFCS-MPC of A Three-phase Cascaded H5 Inverter System

The three-phase cascaded H5 system considered in this research work is shown in Fig. 3(c). It consists of one single-phase H5 inverter in each phase connected to a single-phase utility grid via an inductive filter L_f. The differential equations of the currents in each leg for the three-phase cascaded H5 system in Fig. 3(c) are

$$v_{an} = v_{L_{fa}} + e_a \quad (15a)$$
$$v_{bn} = v_{L_{fb}} + e_b \quad (15b)$$
$$v_{cn} = v_{L_{fc}} + e_c \quad (15c)$$

$$v_{an} = L_{fa}\frac{di_{fa}}{dt} + e_a \quad (16a)$$
$$v_{bn} = L_{fb}\frac{di_{fb}}{dt} + e_b \quad (16b)$$
$$v_{cn} = L_{fc}\frac{di_{fc}}{dt} + e_c \quad (16c)$$

where v_{an}, v_{bn}, and v_{cn} are the voltages across the output of H5 inverter and utility grid of each phase. $v_{L_{fa}}$, $v_{L_{fb}}$, and $v_{L_{fc}}$ are the inductance voltages while e_a, e_b, and e_c are the utility grid voltages of phases a, b, and c, respectively. The voltages across each H5 and utility grid in term of H5 inverters' output voltages are

$$v_{an} = v_{aN} + v_{Nn} \quad (17a)$$
$$v_{bn} = v_{bN} + v_{Nn} \quad (17b)$$
$$v_{cn} = v_{cN} + v_{Nn} \quad (17c)$$

where v_{aN}, v_{bN}, and v_{cN} are the output voltage of H5 inverters of phases a, b, and c. v_{Nn} is the common-mode voltage (v_{cm}) which is defined as

$$v_{cm} = \frac{1}{3}(v_{aN} + v_{bN} + v_{cN}) \quad (18)$$

In three-phase systems, MPC can be implemented either in abc or $\alpha\beta$ reference frames. In this work, AFCS-MPC for a three-phase cascaded H5 inverter system is implemented in $\alpha\beta$ frames since it reduces the computational operations by controlling two variables instead of three Babqi (2018). The three-phase systems can be transformed to $\alpha\beta$ reference frames through Clarke's transformation

Table 2. H7 inverter operation modes

Mode	S_1	S_3	S_5	S_7	V_i
1	0	0	0	0	0
2	0	0	1	1	$\frac{2}{3}V_{dc}\ \angle 0°$
3	0	1	1	1	$\frac{2}{3}V_{dc}\ \angle 60°$
4	0	1	0	1	$\frac{2}{3}V_{dc}\ \angle 120°$
5	1	1	0	1	$\frac{2}{3}V_{dc}\ \angle 180°$
6	1	0	0	1	$\frac{2}{3}V_{dc}\ \angle 240°$
7	1	0	1	1	$\frac{2}{3}V_{dc}\ \angle 300°$
8	1	1	1	0	0

$$\begin{bmatrix}\alpha\\ \beta\end{bmatrix} = \frac{2}{3}\begin{bmatrix}1 & \frac{-1}{2} & \frac{-1}{2}\\ 0 & \frac{\sqrt{3}}{2} & -\frac{\sqrt{3}}{2}\end{bmatrix}\begin{bmatrix}a\\ b\\ c\end{bmatrix} \tag{19}$$

using (19), the equations in (16) can be represented in $\alpha\beta$ as Cortés et al. (2010)

$$v_{\alpha\beta} = L_f \frac{di_{f\alpha\beta}}{dt} + e_{\alpha\beta} \tag{20}$$

where $v_{\alpha\beta}$ are the inverter voltage vectors and $i_{f\alpha\beta}$ are the currents flow between the inverters and utility grids. To predict the future value of $i_{f\alpha\beta}$, (2) is used to obtain the discrete-time model of (20) as

$$i_{f\alpha\beta}(k+1) = i_{f\alpha\beta}(k) + \frac{T_s}{L_f}(v_{i\alpha\beta}(k) - e_{\alpha\beta}(k)) \tag{21}$$

Similar to the single-phase H5 inverter control technique in the previous section, two cost functions are used during the controlling process (22) and (23). In case of dynamics changing of the reference value, the controller predicts the first step (21), and the cost function (22) is used. In steady-state situations the controller predicts a further step (e.g. $i_{f\alpha\beta}(k+2)$, $i_{f\alpha\beta}(k+3)$, ..., or $i_{f\alpha\beta}(k+n)$) and (23) is used. To predict a longer step of the controlled variable, one can follow the same procedure in (14).

$$J = (i^*_\alpha(k{+}1) - i_{f\alpha}(k{+}1))^2 + (i^*_\beta(k{+}1) - i_{f\beta}(k{+}1))^2 \tag{22}$$

$$J = (i^*_\alpha(k{+}n) - i_{f\alpha}(k{+}n))^2 + (i^*_\beta(k{+}n) - i_{f\beta}(k{+}n))^2 \tag{23}$$

3.3 AFCS-MPC of A Three-phase H7 Inverter

The idea of the three-phase H7 inverter Fig. 3(b) is similar to the one of the H5 inverter by adding one more switch for the conventional three-phase two-level inverter Freddy et al. (2014). The additional switch provides galvanic isolation by disconnecting the DC source from the system during the zero voltage vectors. The space vector modulation (SVM) of H7 is shown in table 2. The table shows the top switches $S1$, $S3$, and $S5$ SVM pattern while the bottom ones are switch complimentary. The added switch $S7$ is always closed except with zero voltage vectors. The load currents dynamics in Fig. 3(b) can be described as

$$v_{ia,2} = v_{L_{fa,2}} + Ri_{fa,2} + e_{a,2} \tag{24a}$$
$$v_{ib,2} = v_{L_{fb,2}} + Ri_{fb,2} + e_{b,2} \tag{24b}$$
$$v_{ic,2} = v_{L_{fc,2}} + Ri_{fc,2} + e_{c,2} \tag{24c}$$

$$v_{ia,2} = L_{fa,2}\frac{di_{fa,2}}{dt} + Ri_{fa,2} + e_{a,2} \tag{25a}$$
$$v_{ib,2} = L_{fb,2}\frac{di_{fb,2}}{dt} + Ri_{fb,2} + e_{b,2} \tag{25b}$$
$$v_{ic,2} = L_{fc,2}\frac{di_{fc,2}}{dt} + Ri_{fc,2} + e_{c,2} \tag{25c}$$

where $v_{i,2}$ is the output voltage of the H7 inverter while $v_{L,2}$ is the inductive voltage. e_2 is the utility grid voltage. The equations in (25) can be represented in $\alpha\beta$ reference frames using (19) as

$$v_{i\alpha\beta,2} = L_{f,2}\frac{di_{f\alpha\beta,2}}{dt} + Ri_{f\alpha\beta,2} + e_{\alpha\beta,2} \tag{26}$$

Using (2), the discrete-time model of (26) is

$$\begin{aligned} i_{f\alpha\beta,2}(k+1) =& (1 - \frac{RT_s}{L_f,2})i_{f\alpha\beta,2}(k) + \\ & \frac{T_s}{L_f,2}(v_{i\alpha\beta,2}(k) - e_{\alpha\beta,2}(k)) \end{aligned} \tag{27}$$

The cost functions (22) and (23) can also be used with AFCS-MPC for the three-phase H7 inverter. Therefore, when the difference between the reference and actual values is large, the controller predicts the first step, and (22) is used. On the other hand, at steady-state moments, the controller predicts a longer step, and (23) is used. The cost functions evaluate each voltage vector in table 2 and choose the optimal voltage vector that results in the lowest error value. After that, a combination of switching signals corresponding to the optimal vector is sent to the H7 inverter.

4. SIMULATION RESULTS

The proposed AFCS-MPC control strategy was simulated to examine its performance compared with conventional FCS-MPC. Three different current control case studies were conducted via PSCAD/EMTDC platform, version 4.5 Manitoba (2005), for the three studied inverters typologies. Both AFCS-MPC and FCS-MPC were coded using Fortran and implemented in PSCAD/EMTDC. The studied three inverters which are single-phase H5, three-phase cascaded H5, and three-phase H7 inverters are shown in Fig. 3 while the parameters' values are provided in table 3. The sampling frequencies for both AFCS-MPC and FCS-MPC were set to 33.33 kHz in all cases. The AFCS-MPC was set to predict the 6^{th} step prediction (i.e., $i_f(k+6)$) if the difference between the reference and actual value is less than 200 A. On the other hand, if the difference is more than 200 A, AFCS-MPC will implement the first step prediction (i.e. $i_f(k+1)$) similar to the conventional FCS-MPC.

To compare the proposed control strategy with the conventional FCS-MPC in controlling grid-connected inverter output current, the current reference values were set to 500 A for all the three studied inverters as shown in Fig.

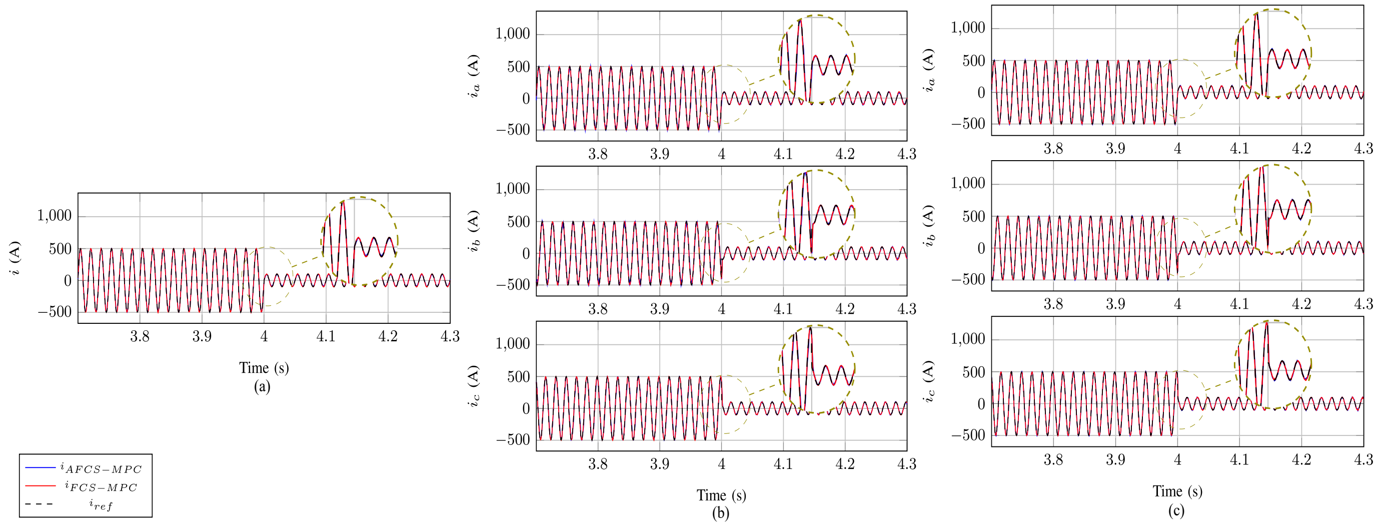

Fig. 4. Output current of: (a) single-phase H5, (b) three-phase cascaded H5, and (c) three-phase H7.

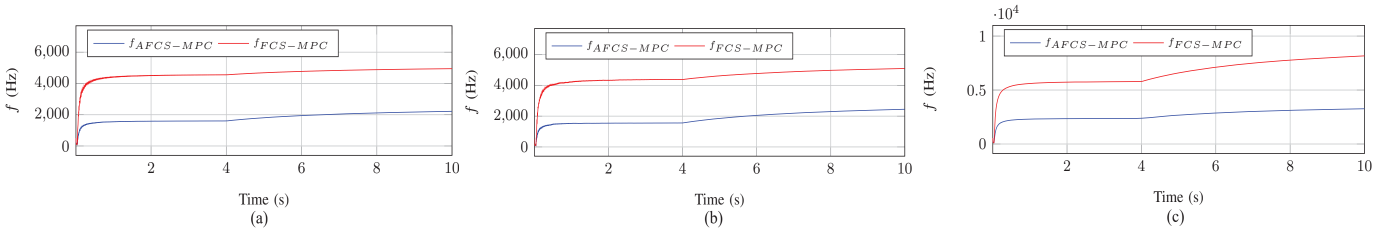

Fig. 5. Average switching frequency during current control of: (a) single-phase H5, (b) three-phase cascaded H5, and (c) three-phase H7.

Table 3. Inverters' parameters in this study.

Parameter	Symbol	Value
DC-link Voltage	V_{PV}	1 KV
Rated Frequency	f_{rated}	60 Hz
Filter Inductance	$L_{f,1}$, L_f , $L_{f,2}$	5, 5, 2 mH
Grid Voltage	$e1, ea, eb, ec$	220 $V_{\text{L-G, RMS}}$
Grid Voltage	$e2$	380 $V_{\text{L-L, RMS}}$

4. The figure shows the output current waveform of H5, three-phase cascaded H5, and H7 during current control using both the AFCS-MPC and FCS-MPC. It can be seen that both controllers follow the reference values with almost similar steady-state responses. In order to evaluate the dynamic response of the proposed control algorithm, the reference current values were changed from 500 A to 100 A for all three inverters at $t = 4$ s. In fact, the proposed algorithm scheme presents the same fast dynamic response as the conventional FCS-MPC. As shown in Fig. 4, the output current values of the H5, cascaded H5, and H7 inverters changed from 500 A to 100 A without any overshoot or delay.

The average switching frequencies of the H5, three-phase cascaded H5, and H7 are shown in Fig. 5. When the reference current was 500 A (e.g., at $t = 2$ s.), the conventional FCS-MPC produced an almost 4.5 kHz average switching frequency during single-phase H5 current control. On the other hand, AFCS-MPC resulted in 1.5 kHz which means that the proposed method reduced the average switching frequency by almost 2/3. When the reference value decreased to 100 A, AFCS-MPC also reduced the switching frequency by around 57%. Similar to the single-phase H5, the proposed control strategy reduces the average switching frequency of the three-phase cascaded H5 inverter by almost the same percentage reduction. For the three-phase H7 inverter, AFCS-MPC reduced the average switching frequency by 60% compared to the conventional method.

As it is expected that AFCS-MPC may result in increasing the output current harmonics since it reduces the average switching frequency. Fig. 6 shows the output currents total harmonic distortion (THD) percentage of the three studied inverters during the grid-connected current control. It can be seen that the proposed AFCS-MPC produces total harmonic distortion higher than the conventional method. However, this increase, which is about 1.3%, is acceptable compared to the merits it brings, and it will not deteriorate the performance of the proposed method.

To further illustrate the effect of the longer prediction steps, Table 4 compares the FCS-MPC with different prediction steps. The table presents each step's output currant's THD and the average switching frequency of each inverter while the reference current was set to 500 A.

5. CONCLUSION

In order to reduce the average switching frequency of the FCS-MPC in PV inverters control, an adaptive finite control set model predictive control for transformerless PV inverters is proposed in this work. The conventional FCS-MPC predicts a predefined and fixed future step of the controlled variables in any situation. On the contrary,

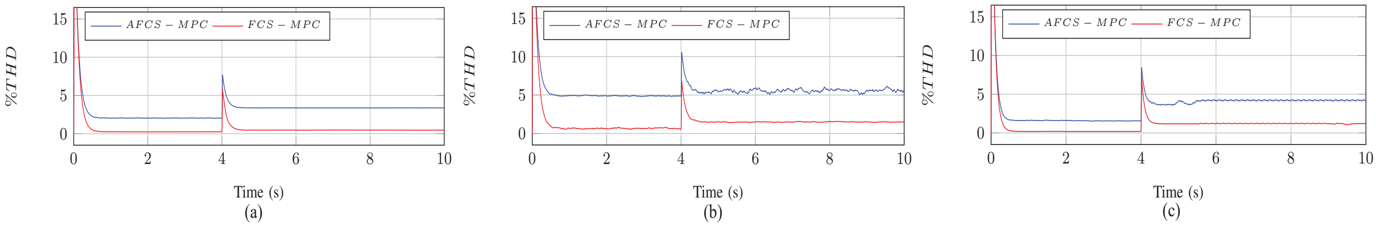

Fig. 6. Output current total harmonic distortion during current control of: (a) single-phase H5, (b) three-phase cascaded H5 (phase a), and (c) three-phase H7 (phase a).

Table 4. Comparison between total harmonics distortion and average switching frequency of different prediction steps.

Step	Single-phase H5		Three-phase cascaded H5		Three-phase H7	
	THD%	*f* (kHz)	*THD%*	*f* (kHz)	*THD%*	*f* (kHz)
1st	0.26	4.50	0.60	4.40	0.21	5.80
2nd	0.50	2.10	1.80	1.95	0.35	2.57
3rd	0.80	1.75	2.60	1.88	0.55	2.40
4th	1.20	1.70	3.50	1.86	0.91	2.35
5th	1.80	1.60	4.10	1.84	1.00	2.32
6th	2.00	1.58	4.90	1.79	1.20	2.30

AFCS-MPC senses the difference between the reference and controlled variables, and dynamically changes the prediction step horizon length to achieve a more economic switching. A comparison between FCS-MPC and AFCS-MPC for controlling the output currents of grid-connected single-phase H5, three-phase cascaded H5, and three-phase H7 inverters was conducted. The simulation results show that AFCS-MPC presents dynamic and steady-state resonances similar to the conventional FCS-MPC. For the cases of controlling the output current of the single-phase H5 and three-phase cascaded H5 inverters, AFCS-MPC reduces the average switching frequency by more than 2/3 for the high reference values while it reduces the switching frequency by 57% in the case of low reference values. In controlling the three-phase H7 inverter, AFCS-MPC reduces the switching frequency by almost 60%. Finally, AFCS-MPC presents a very slight increase in the THD which is related to the average switching frequency.

ABBREVIATIONS AND ACRONYMS

AFCS-MPC Adaptive finite control set model predictive control
FCS-MPC Finite control set model predictive control
PV solar photovoltaic
PSCAD Power System Computer Aided Design
EMTDC Electromagnetic transients including DC
RESs Renewable energy sources
PEDs Power electronics devices
CMV Common-mode voltage
POI Point of interconnection
MPC Model predictive control
KVL Kirchhoffs Voltage Law
SVM Space vector modulation
THD Total harmonic distortion

REFERENCES

Babqi, A.J. and Alamri, B. (2021). A comprehensive comparison between finite control set model predictive control and classical proportional-integral control for grid-tied power electronics devices. *Acta Polytechnica Hungarica*, 18(7), 67–87.

Babqi, A.J. and Etemadi, A.H. (2017). MPC-based microgrid control with supplementary fault current limitation and smooth transition mechanisms. *IET Generation, Transmission & Distribution*, 11(9), 2164–2172.

Babqi, A.J., Yi, Z., Shi, D., and Zhao, X. (2018). Model predictive control of H5 inverter for transformerless PV systems with maximum power point tracking and leakage current reduction. *IECON 2018-44th Annual Conference of the IEEE Industrial Electronics Society*, 1860–1865.

Babqi, A.J. (2018). Finite control set model predictive control for multiple distributed generators microgrids. *Thesis (Ph.D.)–The George Washington University*, (AAT 10684497; ISBN: 9780355515435).

Cortes, P., Rodriguez, J., Silva, C., and Flores, A. (2011). Delay compensation in model predictive current control of a three-phase inverter. *IEEE Transactions on Industrial Electronics*, 59(2), 1323–1325.

Cortes, P., Rodriguez, J., Vazquez, S., and Franquelo, L.G. (2010). Predictive control of a three-phase UPS inverter using two steps prediction horizon. *2010 IEEE International Conference on Industrial Technology*, 1283–1288.

Cortés, P., Wilson, A., Kouro, S., Rodriguez, J., and Abu-Rub, H. (2010). Model predictive control of multilevel cascaded H-bridge inverters. *IEEE Transactions on Industrial Electronics*, 57(8), 2691–2699.

Freddy, T.K.S., Rahim, N.A., Hew, W.P., and Che, H.S. (2014). Modulation techniques to reduce leakage current in three-phase transformerless H7 photovoltaic inverter. *IEEE Transactions on Industrial Electronics*, 62(1), 322–331.

Geyer, T. (2011). A comparison of control and modulation schemes for medium-voltage drives: Emerging predictive control concepts versus PWM-based schemes. *IEEE Transactions on Industry Applications*, 47(3), 1380–1389.

Geyer, T. and Quevedo, D.E. (2014). Performance of multistep finite control set model predictive control for power electronics. *IEEE Transactions on power electronics*, 30(3), 1633–1644.

Guo, X., Zhou, J., He, R., Jia, X., and Rojas, C.A. (2017). Leakage current attenuation of a three-phase cascaded inverter for transformerless grid-connected PV systems. *IEEE Transactions on Industrial Electronics*, 65(1), 676–686.

Hou, C.C., Shih, C.C., Cheng, P.T., and Hava, A.M. (2012). Common-mode voltage reduction pulsewidth modulation techniques for three-phase grid-connected converters. *IEEE transactions on Power Electronics*, 28(4), 1971–1979.

Hu, J., Zhu, J., and Dorrell, D.G. (2014). Model predictive control of grid-connected inverters for PV systems with flexible power regulation and switching frequency reduction. *IEEE Transactions on Industry Applications*, 51(1), 587–594.

Huang, T.G., Sicun, Long, Xun, Xie, and Le (2021). A neural lyapunov approach to transient stability assessment in interconnected microgrids. *Proceedings of the 54th Hawaii International Conference on System Sciences*, 1–10. doi:10.24251/HICSS.2021.405.

Jafarian, H., Bhowmik, S., and Parkhideh, B. (2018). Hybrid current-/voltage-mode control scheme for distributed AC-stacked PV inverter with low-bandwidth communication requirements. *IEEE Transactions on Industrial Electronics*, 65(1), 321–330. doi: 10.1109/TIE.2017.2714129.

Jung, W.s., Choo, K.m., Kim, J.c., Kim, W.j., and Won, C.y. (2018). H7 inverter using zener diode with model predictive current control for common-mode voltage reduction in PMSM drive system. *2018 IEEE International Power Electronics and Application Conference and Exposition (PEAC)*, 1–6.

Kouro, S., Cortés, P., Vargas, R., Ammann, U., and Rodríguez, J. (2008). Model predictive control—A simple and powerful method to control power converters. *IEEE Transactions on industrial electronics*, 56(6), 1826–1838.

Kumar, K.S., Kirubakaran, A., and Subrahmanyam, N. (2020). Bidirectional clamping-based H5, heric, and H6 transformerless inverter topologies with reactive power capability. *IEEE Transactions on Industry Applications*, 56(5), 5119–5128.

Kwak, S. and Mun, S.k. (2014). Model predictive control methods to reduce common-mode voltage for three-phase voltage source inverters. *IEEE Transactions on Power Electronics*, 30(9), 5019–5035.

Li, H., Zeng, Y., Zhang, B., Zheng, T.Q., Hao, R., and Yang, Z. (2018). An improved H5 topology with low common-mode current for transformerless PV grid-connected inverter. *IEEE Transactions on Power Electronics*, 34(2), 1254–1265.

Li, X., Shadmand, M.B., Balog, R.S., and Rub, H.A. (2015). A harmonic constrained minimum energy controller for a single-phase grid-tied inverter using model predictive control. *2015 IEEE Energy Conversion Congress and Exposition (ECCE)*, 5153–5159.

Long, X., Parent, W., and Staff, E. (2015). Influence of power quality on FortisAlberta's PLC based Automatic Meter Reading system. *2015 IEEE Electrical Power and Energy Conference (EPEC)*, 164–168. doi: 10.1109/EPEC.2015.7379944.

Manitoba, H. (2005). PSCAD-Power Systems Computer Aided Design: User's Guide. *Manitoba HVDC Research Centre*.

Naeem, A. and Hassan, N.U. (2020). Renewable energy intermittency mitigation in microgrids: State-of-the-art and future prospects. *2020 4th International Conference on Green Energy and Applications (ICGEA)*, 158–164.

Nassif, A. and Long, X. (2016). Mitigating overvoltage scenarios caused by large penetration of distributed energy resources. *2016 IEEE Electrical Power and Energy Conference (EPEC)*, 1–5. doi:10.1109/EPEC.2016.7771699.

Nikoletatos, J. and Tselepis, S. (2015). Renewable energy integration in power grids: Technology brief. *IEA-ETSAP and IRENA, Tech. Rep.*

Ranalder, L., Busch, H., Hansen, T., Brommer, M., Couture, T., Gibb, D., Guerra, F., Nana, J., Reddy, Y., Sverrisson, F., et al. (2020). Renewables in Cities 2021 Global Status Report.

Rodriguez, J., Pontt, J., Silva, C.A., Correa, P., Lezana, P., Cortés, P., and Ammann, U. (2007). Predictive current control of a voltage source inverter. *IEEE transactions on industrial electronics*, 54(1), 495–503.

Rodriguez, J. and Cortes, P. (2012). Predictive control of power converters and electrical drives. *John Wiley & Sons*, 40.

Rodriguez, J., Kazmierkowski, M.P., Espinoza, J.R., Zanchetta, P., Abu-Rub, H., Young, H.A., and Rojas, C.A. (2012). State of the art of finite control set model predictive control in power electronics. *IEEE Transactions on Industrial Informatics*, 9(2), 1003–1016.

Sangsefidi, Y., Ziaeinejad, S., and Mehrizi-Sani, A. (2016). Low switching frequency-based predictive control of a grid-connected voltage-sourced converter. *IEEE Transactions on Energy Conversion*, 32(2), 686–697.

Shayestegan, M. (2018). Overview of grid-connected two-stage transformer-less inverter design. *Journal of Modern Power Systems and Clean Energy*, 6(4), 642–655. doi:10.1007/s40565-017-0367-z.

Vargas, R., Rodriguez, J., Rojas, C.A., and Rivera, M. (2014). Predictive control of an induction machine fed by a matrix converter with increased efficiency and reduced common-mode voltage. *IEEE Transactions on Energy Conversion*, 29(2), 473–485.

Victor, M., Greizer, F., Bremicker, S., and Hübler, U. (2008). Method of converting a direct current voltage from a source of direct current voltage, more specifically from a photovoltaic source of direct current voltage, into a alternating current voltage. US Patent 7,411,802.

Wang, Y., Yi, Z., Shi, D., Yu, Z., Huang, B., and Wang, Z. (2018). Optimal distributed energy resources sizing for commercial building hybrid microgrids.

Xie, X., Sun, Y., Long, X., and Zhang, B. (2017). A new method to monitor the primary neutral integrity in multi-grounded neutral systems. *Energies*, 10(3). doi: 10.3390/en10030380.

Yi, Z., Babqi, A.J., Wang, Y., Shi, D., Etemadi, A.H., Wang, Z., and Huang, B. (2018). Finite-control-set model predictive control (FCS-MPC) for islanded hybrid microgrids. *2018 IEEE Power Energy Society General Meeting (PESGM)*, 1–5. doi: 10.1109/PESGM.2018.8586292.

Yi, Z. and Etemadi, A.H. (2017). Fault detection for photovoltaic systems based on multi-resolution signal decomposition and fuzzy inference systems. *IEEE Transactions on Smart Grid*, 8(3), 1274–1283. doi: 10.1109/TSG.2016.2587244.

Yi, Z., Zhao, X., Shi, D., Duan, J., Xiang, Y., and Wang, Z. (2019). Accurate power sharing and synthetic inertia control for DC building microgrids with guaranteed performance. *IEEE Access*, 7.